Modal Analysis of the Orion Capsule Two Parachute System

J. Pei[1], C. Roithmayr[1], R. Barton[2], D. Matz[3], J. Beaty[4], [1]NASA Langley Research Center, Hampton VA 23681. [2]Retired. NASA Johnson Space Flight Center, Houston TX 77058. [3]NASA Johnson Space Flight Center, Houston TX 77058. [4]Retired. NASA Langley Research Center, Hampton VA 23681.

Brief Presenter Biography: Jing Pei works in the Vehicle Analysis Branch at NASA Langley Research Center and is a member of NASA's Engineering and Safety Center (NESC) flight mechanics technical discipline team. His interests include: atmospheric flight mechanics, orbital dynamics, Guidance Navigation & Control, modeling and simulation for launch vehicles, aircraft, UAVs, spacecraft, and re-entry systems.

Introduction: As discussed in Ref [1], it is apparent from flight tests that the system made up of two main parachutes and a capsule can undergo several distinct dynamical behaviors. The most significant and problematic of these is the pendulum mode in which the system develops a pronounced swinging motion with an amplitude of up to 24 deg. Large excursions away from vertical by the capsule could cause it to strike the ground at a large horizontal or vertical speed and jeopardize the safety of the astronauts during a crewed mission. In reference [1], Ali et al. summarized a series of efforts taken by the Capsule Parachute Assembly System (CPAS) Program to understand and mitigate the pendulum issue. The period of oscillation and location of the system's pivot point are determined from post-flight analysis [2].

Other noticeable but benign modes include: 1) flyout (scissors) mode, where the parachutes move back and forth symmetrically with respect to the vertical axis similar to the motion of a pair of scissors; 2) maypole mode, where the two parachutes circle around the vertical axis at a nearly constant radius and period; and 3) breathing mode, in which deformation of the non-rigid canopies affects the axial acceleration of the system in an oscillatory manner. Because these modes are relatively harmless, little effort has been devoted to analyzing them in comparison with the pendulum motion.

Motions of the actual system made up of two parachutes and a capsule are extremely complicated due to nonlinearities and flexibility effects. Often it is difficult to obtain insight into the fundamental dynamics of the system by examining results from a multi-body simulation based on nonlinear equations of motion (EOMs). As a part of this study, the dynamics of each mode observed during flight is derived from first principles on an individual basis by making numerous simplifications along the way. The intent is to gain a better understanding into the behavior of the complex multi-body system by studying the reduced set of differential equations associated with each mode. This approach is analogous to the traditional modal analysis technique used to study airplane flight dynamics [3], in which the full nonlinear behavior of the airframe is decomposed into the phugoid and short period modes for the longitudinal dynamics and the spiral, roll-subsidence, and dutch-roll modes for the lateral dynamics. It is important to note that the study does not address the mechanisms that cause the system to transition from one mode to another, nor does it discuss motions during which two or more modes occur simultaneously.

Pendulum Mode: Over the past 50 years, a number of analytical, numerical, and experimental investigations have been performed with the goal of understanding parachute pitch-plane dynamics (e.g., refs. [4]–[6]). Reference [7] used computational fluid dynamics (CFD) to study the stability of various main parachute configurations from the Apollo and Multi-Purpose Crew Vehicle (MPCV) Programs. It was demonstrated that an increase in the porosity of the parachute improved its stability characteristics, and hence reduce the severity of the pendulum motion. Figure 1 shows representative plots of C_N and C_A comparing a stable versus an unstable main parachute configuration. It is apparent from the C_N versus α plot that the unstable configuration has a negative slope at $\alpha = 0$ and two stable equilibrium points at $\pm\alpha_o$. As described in ref. [7], by adding a "gap" in the parachute (increased porosity), the C_N slope becomes close to zero at $\alpha = 0$ and is considered the stable configuration. In addition, the two stable α_o shift closer to $\alpha = 0$. However, this modification comes at a cost in the reduction of the C_A, which results in a higher descent velocity. References [6] and [8] provide similar insights regarding the flow physics associated with non-porous and porous configurations and how these affect the parachute stability characteristics. The current study focuses on the unstable MPCV main parachute design (modeled by the red curves in Figure 1), which is highly susceptible to the pendulum motion under the two-main cluster configuration.
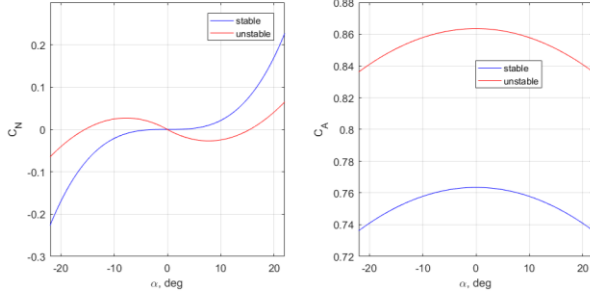
Figure 1. C_N and C_A Coefficients Representative of Unstable versus Stable Parachute Configurations

The planar dumbbell model used to study the underlying dynamics of the pendulum motion is illustrated in Figure 2. The capsule is modeled as a particle rather than an extended rigid body, and aerodynamic forces acting on the capsule are ignored [4]. The two parachutes are treated as a single particle. The rigid body B contains two particles. Particle P_C has a mass of m_C, the total mass of two parachutes, which includes dry mass as well as the mass of air trapped in each of the canopies. Particle P_L has a mass of m_L and represents the capsule. Body B moves such that P_C and P_L remain at all times in a plane fixed in a Newtonian reference frame N. A right-handed set of mutually perpendicular unit vectors n_1, n_2, and n_3 is fixed in N. Unit vectors n_1 and n_3 lie in the plane in which motion takes place, and are directed as shown in Figure 2; n_1 is horizontal, n_2 is directed into the page, and n_3 is vertical, directed downward. A right-handed set of mutually perpendicular unit vectors b_1, b_2, and b_3 is fixed in B. Unit vectors b_1 and b_3 are directed as shown in Figure 2; b_1 has the same direction as the position vector $\mathbf{r}^{P_C P_L}$ from P_C to P_L. Unit vector b_2 is directed into the page; note that it is fixed in N as well as in B.
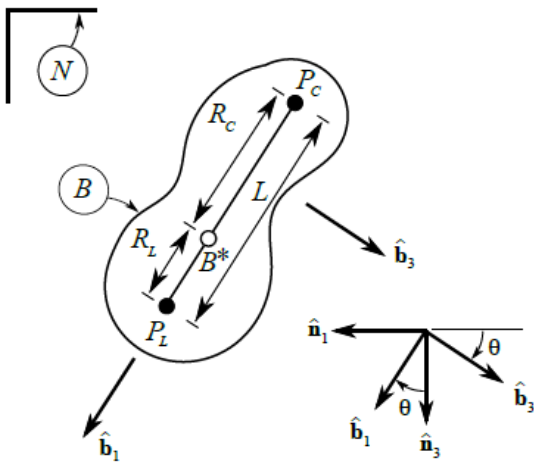

Figure 2. Dumbbell Model for Pendulum Motion

The following two relationships governing translation and rotation of the dumbbell are derived in reference [9]:

$$^{N}\boldsymbol{a}^{B*} = \frac{1}{m_C + m_L}\{-[A_x \sin\theta + A_z \cos\theta]n_1 + $$
$$[W_C + W_L - A_x \cos\theta + A_z \sin\theta]n_3\} \qquad (1)$$

$$\ddot{\theta} + \frac{1}{m_C L}[(m_C\, g - W_C)\sin\theta - A_z] = 0 \qquad (2)$$

where $W_L = m_L\, g$ and g is the magnitude of the local gravitational force per unit of mass. W_C is the sum of the dry weights of the two parachutes; the weight of the air trapped in their canopies is ignored because the gravitational force exerted on that air is assumed to be counteracted by buoyancy effects from the ambient atmosphere. A_x, the magnitude of the resultant of the aerodynamic axial forces applied to the two parachutes, can be expressed as:

$$A_x = 2q_\infty S_{\mathrm{ref}} C_A \qquad (3)$$

where q_∞ is the dynamic pressure, S_{ref} is the reference area of a single parachute, and C_A is the drag coefficient for a single parachute. The absolute value of A_z is the magnitude of the resultant of the aerodynamic normal forces applied to the two parachutes; A_z can be expressed as:

$$A_z = -2q_\infty S_{\mathrm{ref}} C_N \qquad (4)$$

where C_N is the aerodynamic normal force coefficient for a single parachute. As discussed in references [4] and [5], C_A and C_N are nonlinear functions of α, the instantaneous angle of attack of the parachute:

$$C_A(\alpha) = C_{A_o} + \frac{1}{2}C_{A_\alpha}\alpha_0\left(\frac{\alpha^2}{\alpha_0{}^2} - 1\right) \qquad (5)$$

$$C_N(\alpha) = \frac{C_{N_\alpha}}{2\alpha_0^2}(\alpha^3 - \alpha_0{}^2\alpha) \qquad (6)$$

Here, α_0 is the stable trim angle of attack and C_{N_α} is the slope of the C_N curve at α_0. An additional damping term $C_{N_{\dot\alpha}}$ was added to Eq. (6) to account for unsteady time lag effects in the rotational DOF ref. [3] and [11].

Much insight into the stability of the parachutes can be obtained by assuming that C_N is a linear function of α in the neighborhood of a stable equilibrium point, α_o. For small-amplitude oscillations, the rotational equation of motion is found to have the form of the second-order linear differential equation governing damped, free vibrations, and a general solution of the differential equation is given. A point on the dumbbell whose trajectory is nearly a straight line for undamped, small-amplitude oscillations is identified. The distance from this pivot point to the capsule is of interest because the capsule

moves as though that distance is the length of a simple pendulum. In the case of a simple pendulum, the length of the string between the pivot point and pendulum bob determines the distance traveled by the bob on a circular arc as the pendulum swings. The length of the string also determines the period of oscillations. Analogously, the distance from the pivot point to the capsule is an important parameter in capsule-parachute pendulum motion. When this distance is minimized, undesirable swinging motion of the capsule is also minimized.

When θ remains small, Eq. (2) can be approximated as

$$\ddot{\theta} + \frac{W_{\text{tot}}}{m_C L C_A}(C_{N_{\dot{\alpha}}})_{\text{tot}}\,\dot{\theta} + \frac{1}{m_C L}\Big[(m_C\,g - W_C) + \frac{W_{\text{tot}}}{C_A}C_{N_{\alpha}}\Big]\theta = 0 \tag{7}$$

This second-order linear differential equation has the form

$$\ddot{x} + 2b\dot{x} + \omega_n{}^2 x = 0 \tag{8}$$

which governs damped free vibrations. ω_n is referred to as the circular natural frequency, and b/ω_n is the fraction of critical damping, or damping ratio. We define b and $\omega_n{}^2$ as:

$$b = \frac{W_{\text{tot}}}{2m_C L C_A}(C_{N_{\dot{\alpha}}})_{\text{tot}} \tag{9}$$

and

$$\omega_n{}^2 = \frac{1}{m_C L}\Big[(m_C\,g - W_C) + \frac{W_{\text{tot}}}{C_A}C_{N_{\alpha}}\Big] \tag{10}$$

The general solution of Eq. (7) is then given by

$$\theta = e^{-bt}[C_1\sin(\omega_d\,t) + C_2\cos(\omega_d\,t)] \tag{11}$$

where the damped natural frequency, ω_d, is given by

$$\omega_d = \sqrt{\omega_n{}^2 - b^2} \tag{12}$$

and the constants C_1 and C_2 can be expressed in terms of the initial values $\theta_0 = \theta(t = 0)$ and $\dot{\theta}_0 = \dot{\theta}(t = 0)$,

$$C_1 = \frac{1}{\omega_d}\big(\dot{\theta}_0 + b\theta_0\big) \tag{13}$$

$$C_2 = \theta_0 \tag{14}$$

The constants appearing in the fraction on the right-hand side of Eq. (9) are all positive; therefore, the sign of b is determined by the sign of $(C_{N_{\dot{\alpha}}})_{\text{tot}}$. Exponential decay in θ occurs for $(C_{N_{\dot{\alpha}}})_{\text{tot}} > 0$, whereas there is exponential growth in θ for $(C_{N_{\dot{\alpha}}})_{\text{tot}} < 0$. In either case, the damped frequency ω_d of oscillations in θ is smaller than ω_n; consequently, the period of damped oscillations is larger than that of undamped oscillations.

Solutions of dynamical equations governing planar motions of the dumbbell reveal the existence of a point Q, on the line joining P_L and P_C, whose trajectory in N is very nearly a straight line; from this observation, it can be inferred that the magnitude of the acceleration ${}^N a^Q$ of Q in N is nearly zero. In what follows, we find the distance L_L from P_L to Q such that ${}^N a^Q \cdot b_3 = 0$ for undamped oscillations having small amplitude. It is also shown that, under the same conditions, ${}^N a^Q \cdot b_1$ is small when the initial values θ_0 and $\dot{\theta}_0$ are zero and small, respectively. Q is referred to as the pivot point; the smaller the value of L_L is, the better the landing conditions will be for the capsule.

The acceleration ${}^N a^Q$ of Q in N is, with the aid of Eq. (1), given by

$$
{}^N \boldsymbol{a}^Q = \Big[\frac{(W_C + W_L)\cos\theta - A_x}{m_C + m_L} + (L_L - R_L)\dot{\theta}^2\Big]b_1 + \Big[\frac{(W_C + W_L)\sin\theta + A_z}{m_C + m_L} + (L_L - R_L)\ddot{\theta}\Big]b_3 \tag{15}
$$

One can determine the value of L_L such that ${}^N a^Q \cdot b_3 = 0$ when θ remains small and oscillations are undamped [9]:

$$
{}^N a^Q \cdot b_3 = \frac{(W_C + W_L)\sin\theta + A_z - m_C L\ddot{\theta}}{m_C + m_L} + L_L\ddot{\theta} = 0 \tag{16}
$$

In view of Eq. (2) and the fact that $W_L = m_L\,g$, we have

$$
\frac{(W_C + W_L)\sin\theta + (m_C\,g - W_C)\sin\theta}{m_C + m_L} + L_L\ddot{\theta} = g\sin\theta + L_L\ddot{\theta} = 0 \tag{17}
$$

Thus, after substitution from Eq. (28) of [9] with $(C_{N_{\dot{\alpha}}})_{\text{tot}} = 0$,

$$
-L_L\ddot{\theta} = \frac{L_L}{m_C L}\Big[(m_C\,g - W_C)\sin\theta + \frac{W_{\text{tot}}}{C_A}C_{N_{\alpha}}\theta\Big] = g\sin\theta \tag{18}
$$

When θ remains small, L_L can be expressed as

$$
L_L = \frac{m_C\,g\,C_A}{(m_C\,g - W_C)C_A + W_{\text{tot}}C_{N_{\alpha}}}\,L \tag{19}
$$

It is easily shown that $L_L = R_L$ when $C_A = C_{N_{\alpha}}$, in which case Q is coincident with B^*. When $C_{N_{\alpha}} = 0$, it

is evident that L_L slightly exceeds L because the numerator in Eq. (19) becomes the sum of the masses of the dry parachutes and entrapped air, whereas the denominator consists only of the masses of entrapped air.

As the distance L_L decreases the pivot point moves closer to the capsule, which decreases the distance the payload travels over a circular path during pendulum motion. Equation (19) is a key relationship for a two-parachute system that substantiates observations made in previous studies of pendulum motion; 1) increasing the parachute C_{N_α} moves the pivot point towards the payload and reduces the distance traveled by the capsule as it swings; 2) decreasing the parachute drag coefficient (by increasing its porosity) moves the pivot point towards the payload and reduces the distance traveled by the capsule as it swings; however, this benefit comes at the expense of increasing the steady-state descent rate, which may not be desirable; 3) decreasing the payload mass (the largest contributor to W_{tot}) shifts the pivot point towards the parachutes and increases the distance traveled by the capsule as it swings, and 4) an increase in the atmospheric density increases the mass of the air entrapped in the canopy (the larger part of m_C) and moves the pivot point towards the parachutes. These observations are consistent with conclusions drawn in Refs. [4], [6], and [7]. Reference [10] describes the global nonlinear behavior of the pendulum motion.

Flyout Mode: Reference [1] describes the flyout, or scissors, motion as two parachutes moving sinusoidally away from or toward the vertical axis in a symmetrical manner, while the capsule descends at nearly constant speed. A simple planar model involving three particles is used to study the underlying dynamics of the scissors motion, as shown in Figure 3. Particle P_L has a mass of m_L and represents the capsule. The two parachutes are treated as identical particles, P_B and P_C; each has a mass of m_C, which includes dry mass as well as the mass of air trapped inside the canopy. The system moves such that the three particles remain at all times in a plane fixed in a Newtonian reference frame N. A right-handed set of mutually perpendicular unit vectors n_1, n_2, and n_3 is fixed in N. Unit vectors n_1 and n_3 lie in the plane in which motion takes place and are directed as shown in Figure 3; n_1 is horizontal, n_2 is directed out of the page, and n_3 is vertical, directed downward. P_B and P_C each are connected to P_L by a massless, rigid link; the two links are connected by a revolute joint whose axis is parallel to n_2. P_B and one link are fixed in a reference frame B, whereas P_C and the other link are fixed in a reference frame C. The orientations of B and C in N are described by angles θ_1 and θ_2, respectively. A dextral set of mutually perpendicular unit vectors b_1, b_2, and b_3

is fixed in B and directed as shown in Figure 3; b_2 is directed out of the page. A similar set of unit vectors c_1, c_2, and c_3 is fixed in C; c_2 is directed into the page. Note that b_2 and c_2 are each fixed in the three reference frames N, B, and C. The resultant external forces acting on P_L, P_B, and P_C are denoted by F_L, F_B, and F_C, respectively.
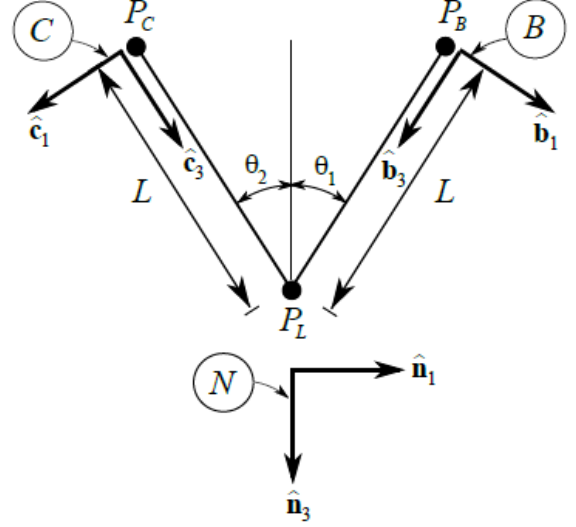

Figure 3. Scissors Mode Planar Model

The equation of motion governing the horizontal speed of P_L, which is not presented, shows that horizontal acceleration of P_L vanishes under the following conditions: $(\mathbf{F}_L + \mathbf{F}_B + \mathbf{F}_C) \cdot \hat{\mathbf{n}}_1 = 0$, $\theta_1 = \theta_2$, $\dot{\theta}_1 = \dot{\theta}_2$, and $\ddot{\theta}_1 = \ddot{\theta}_2$. The latter three conditions simply correspond to the symmetric motion of the parachutes that characterizes the scissors behavior under consideration. In the following, all four conditions are assumed to exist, and the horizontal speed of P_L is taken to be constant and equal to zero. In that case, the three-particle system has three DOFs in N, and three motion variables u_1, u_2, and u_3 are introduced as follows: u_1 is the projection onto $\hat{\mathbf{n}}_3$ of the velocity of P_L in N, $u_2 = \dot{\theta}_1$, and $u_3 = \dot{\theta}_2$. Using Kane's method [Ref. 12], the equations of motion can be written in matrix form as

$$\begin{bmatrix} m_L + 2m_C & m_C L \sin\theta_1 & m_C L \sin\theta_2 \\ m_C L \sin\theta_1 & m_C L^2 & 0 \\ m_C L \sin\theta_2 & 0 & m_C L^2 \end{bmatrix} \begin{Bmatrix} \dot{u}_1 \\ \dot{u}_2 \\ \dot{u}_3 \end{Bmatrix} \quad (20)$$

$$= \begin{Bmatrix} \hat{\mathbf{n}}_3 \cdot (\mathbf{F}_L + \mathbf{F}_B + \mathbf{F}_C) - m_C L(\cos\theta_1 u_2{}^2 + \cos\theta_2 u_3{}^2) \\ L\hat{\mathbf{b}}_1 \cdot \mathbf{F}_B \\ L\hat{\mathbf{c}}_1 \cdot \mathbf{F}_C \end{Bmatrix}$$

The mass matrix is symmetric, as expected. One can, of course, divide the second and third equations by L. Symmetric motion of the parachutes occurs when the magnitude of the normal force $\hat{\mathbf{b}}_1 \cdot \mathbf{F}_B$ applied to P_B is identical to the magnitude of the normal force $\hat{\mathbf{c}}_1 \cdot \mathbf{F}_C$ applied to P_C, the initial values of θ_1 and θ_2 are identical, and the initial values of u_2 and u_3 are identical.

The contribution of aerodynamic forces to $\mathbf{F}_L$ is ignored, and the force can be expressed as

$$\mathbf{F}_L = m_L g \hat{\mathbf{n}}_3 = W_L \hat{\mathbf{n}}_3 \tag{21}$$

The resultant external force applied to P_B is given by

$$\mathbf{F}_B = q_\infty S_{\text{ref}}[-(C_N)_{\text{tot}}\hat{\mathbf{b}}_1 - C_A \hat{\mathbf{b}}_3 + W_C \hat{\mathbf{n}}_3] \tag{22}$$

where W_C is the dry weight of a single parachute. The weight of the air trapped in the canopy is ignored because the gravitational force exerted on that air is assumed to be counteracted by buoyancy effects from the ambient atmosphere. The total normal force coefficient, $(C_N)_{\text{tot}}$, is the sum of the free-stream normal force coefficient, $(C_N)_{\text{fs}}$, and the normal force coefficient due to parachute proximity effects, $(C_N)_{\text{prox}}$:

$$(C_N)_{\text{tot}} = (C_N)_{\text{fs}} + (C_N)_{\text{prox}} \tag{23}$$

As shown in Figure 3 and Equation (23), $(C_N)_{\text{fs}}$ is generally a nonlinear function of α. In general, it is also a function of $\dot{\alpha}$. For this analysis it is assumed that the parachutes are oscillating about some trimmed α. Small angles are assumed, $\theta' \approx \alpha'$, where θ' and α' are deviations about the trimmed θ and α, respectively, and C_N varies linearly with α. $(C_N)_{\text{prox}}$ is a function of D_{prox}, the distance between the parachute centers, and V_{prox}, the time derivative of D_{prox}. Proximity distance can be expressed as $D_{\text{prox}} = 2L \sin \theta$, and its time derivative is, thus, $V_{\text{prox}} = 2L \cos \theta \, \dot{\theta}$. The derivatives of the normal force coefficients have a relationship similar to Equation (23):

$$(C_{N_\alpha})_{\text{tot}} = (C_{N_\alpha})_{\text{fs}} + (C_{N_\alpha})_{\text{prox}} \tag{24}$$

The resultant external force applied to P_C is given by

$$\mathbf{F}_C = q_\infty S_{\text{ref}}[-(C_N)_{\text{tot}}\hat{\mathbf{c}}_1 - C_A \hat{\mathbf{c}}_3] + W_C \hat{\mathbf{n}}_3 \tag{25}$$

If the dynamic coupling in Equations (20) is ignored (valid approximation since the contribution of $\dot{u}_1$ to $\dot{u}_2$ is small), damping is neglected, and θ_1 is assumed to remain small, then the second of Equations (20) describes an undamped harmonic oscillation:

$$\dot{u}_2 = \ddot{\theta}_1 \approx \frac{W_C - q_\infty S_{\text{ref}}(C_{N_\alpha})_{\text{tot}}}{m_C L} \theta_1 \tag{26}$$

The period associated with the scissors motion, T, is found to be inversely proportional to $(C_{N_\alpha})_{\text{tot}}$:

$$T = 2\pi \sqrt{\frac{m_C L}{q_\infty S_{\text{ref}}(C_{N_\alpha})_{\text{tot}} - W_C}} \tag{27}$$

$(C_{N_\alpha})_{\text{tot}}$ can be expressed as a function of T and key system parameters:

$$(C_{N_\alpha})_{\text{tot}} = \frac{1}{q_\infty S_{\text{ref}}}\left(\frac{4\pi^2 m_C L}{T^2} + W_C\right) \tag{28}$$

Maypole Mode: Maypole motion described in Reference [1] consists of two parachutes orbiting about the vertical axis. A simplified model used to study maypole motion is illustrated in Figure 4. The three particles P_L, P_B, and P_C are the same as those described in Fig 3; in the present model, however, all three are assumed to be fixed in a rigid body B. A right-handed set of mutually perpendicular unit vectors b_1, b_2, and b_3 is fixed in B and directed as shown in Figure 4; b_2 is normal to the plane containing P_L, P_B, and P_C; and b_3 is parallel to an axis of symmetry of B, which is therefore a central principal axis of inertia of B. A dextral set of mutually perpendicular unit vectors n_1, n_2, and n_3 is fixed in a Newtonian reference frame N. n_1 is horizontal, n_2 is directed out of the page, and n_3 is vertical, directed downward. B moves in N such that $b_3 = n_3$ at all times. Moreover, the velocity in N of every point on the axis of symmetry of B has the same constant magnitude and the same direction as n_3. Two additional sets of dextral, mutually perpendicular unit vectors are introduced for convenience in conducting kinematic analysis and expressing the forces applied to B. Both sets of unit vectors are fixed in B. The first set contains e_1, e_2, and e_2, whereas the second set contains f_1, f_2, and f_3.
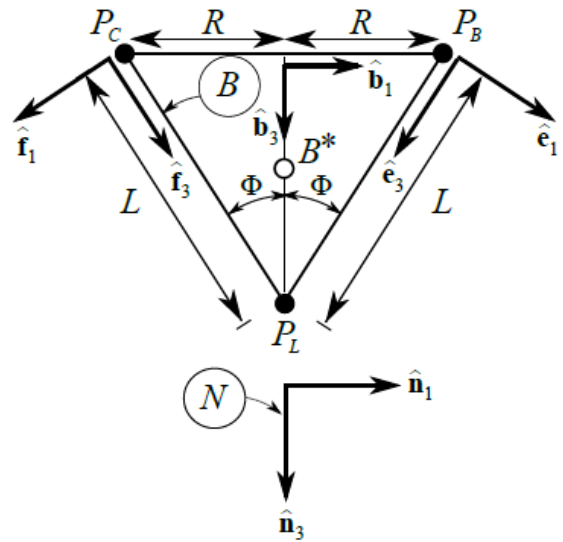

Figure 4. Maypole Mode Model

For example, P_L lies on the axis of symmetry, so the velocity of P_L in N can be written as

$$^N\mathbf{v}^{P_L} = V_3\hat{\mathbf{n}}_3 \qquad (29)$$

where V_3 is a constant. Hence, the acceleration in N of P_L and every point on the axis of symmetry is zero:

$$^N\mathbf{a}^{P_L} = \mathbf{0} \qquad (30)$$

The mass center of B, denoted by B^*, lies on the axis of symmetry and, therefore, has an acceleration in N equal to zero. Based on first principles, this requires that the resultant of all external forces applied to B is equal to zero. The angular velocity $^N\boldsymbol{\omega}^B$ of B in N that characterizes maypole motion is parallel to a central principal axis of inertia of B,

$$^N\boldsymbol{\omega}^B = \Omega\hat{\mathbf{b}}_3 = \Omega\hat{\mathbf{n}}_3 \qquad (31)$$

where Ω is a constant. Thus, the angular acceleration $^N\boldsymbol{\alpha}^B$ of B in N is zero:

$$^N\boldsymbol{\alpha}^B = \mathbf{0} \qquad (32)$$

Euler's rotational equations of motion are satisfied by Equations (31) and (32) only if the resultant moment about B of all external forces applied to B is equal to zero. The accelerations in N of P_B and P_C are then determined to be

$$^N\mathbf{a}^{P_B} = \Omega L \sin\,\Phi\,\Omega\hat{\mathbf{b}}_3 \times \hat{\mathbf{b}}_2 = -R\Omega^2\hat{\mathbf{b}}_1 \quad (33)$$

$$^N\mathbf{a}^{P_C} = -\Omega L \sin\,\Phi\,\Omega\hat{\mathbf{b}}_3 \times \hat{\mathbf{b}}_2 = R\Omega^2\hat{\mathbf{b}}_1 \quad (34)$$

where $R = L\sin\,\Phi$, as indicated in Figure 4.

Two additional sets of dextral, mutually perpendicular unit vectors are introduced for convenience in conducting kinematic analysis and expressing the forces applied to B. Both sets of unit vectors are fixed in B. The first set contains $\hat{\mathbf{e}}_1$, $\hat{\mathbf{e}}_2$, and $\hat{\mathbf{e}}_3$, whereas the second set contains $\hat{\mathbf{f}}_1$, $\hat{\mathbf{f}}_2$, and $\hat{\mathbf{f}}_3$.

The resultants of the external forces acting on P_L, P_B, and P_C are once again denoted by $\mathbf{F}_L$, $\mathbf{F}_B$, and $\mathbf{F}_C$, respectively. $\mathbf{F}_L$ is expressed as

$$\mathbf{F}_L = m_L g\hat{\mathbf{n}}_3 = W_L\hat{\mathbf{n}}_3 \qquad (35)$$

The resultant external force applied to P_B is, in general, given by

$$\mathbf{F}_B = q_\infty S_{\text{ref}}[-(C_N)_{\text{tot}}\hat{\mathbf{e}}_1 + C_Y\hat{\mathbf{e}}_2 \\ - C_A\hat{\mathbf{e}}_3] + W_C\hat{\mathbf{n}}_3 \qquad (36)$$

where W_C is the dry weight of a single parachute. $(C_N)_{\text{tot}}$ can in this case be expressed as in Equation (23). In addition, it is assumed that $\Phi = \alpha$ and the parachutes are in static equilibrium with constant flyout angles and at some trimmed angle of attack α_{trim} while

performing the maypole motion. The resultant external force applied to P_C is similar to F_B:

$$\mathbf{F}_C = q_\infty S_{\text{ref}}[-(C_N)_{\text{tot}}\hat{\mathbf{f}}_1 + C_Y\hat{\mathbf{f}}_2 \\ - C_A\hat{\mathbf{f}}_3] + W_C\hat{\mathbf{n}}_3 \qquad (37)$$

However, the side forces associated with C_Y would yield a nonzero moment about B^* that is parallel to $\hat{\mathbf{b}}_3$. Hence, maypole motion requires

$$C_Y = 0 \qquad (38)$$

Because P_L and P_B are connected by a rigid link, each exerts a force on the other. The force exerted by P_L on P_B can be expressed as $T\hat{\mathbf{e}}_3$. This internal force must be accounted for when applying Newton's second law to P_B; however, forming dot products with $\hat{\mathbf{e}}_1$ will eliminate T. That is,

$$(\mathbf{F}_B + T\hat{\mathbf{e}}_3) \cdot \hat{\mathbf{e}}_1 = \mathbf{F}_B \cdot \hat{\mathbf{e}}_1 \\ = m_C\,^N\mathbf{a}^{P_B} \cdot \hat{\mathbf{e}}_1 \qquad (39)$$

Substitution from Equations (33) and (36) yields

$$\{q_\infty S_{\text{ref}}[-(C_N)_{\text{tot}}\hat{\mathbf{e}}_1 - C_A\hat{\mathbf{e}}_3] + W_C\hat{\mathbf{n}}_3\} \cdot \hat{\mathbf{e}}_1 = \\ -m_C R\Omega^2 \cos\,\Phi \qquad (40)$$

This relationship can be solved for $(C_N)_{\text{tot}}$:

$$(C_N)_{\text{tot}} = \frac{m_C R\Omega^2 \cos\,\Phi + W_C \sin\,\Phi}{q_\infty S_{\text{ref}}} \qquad (41)$$

Thus, the aerodynamic normal force is seen to be directly proportional to the magnitude of the centripetal acceleration of P_B (or P_C). One can also conclude that the radius and period of the maypole mode is dependent on the value of $(C_N)_{\text{tot}}$ at α_{trim}. For a given orbital radius R, the orbital angular rate is given by

$$\Omega = \sqrt{\frac{q_\infty S_{\text{ref}}(C_N)_{\text{tot}} - W_C \sin\,\Phi}{m_C R \cos\,\Phi}} \qquad (41)$$

The orbital period of maypole motion is thus seen to be inversely proportional to $(C_N)_{\text{tot}}$. Finally, by appealing to the fact that the resultant external force applied to B must be $\mathbf{0}$ for maypole motion to take place, a relationship between $(C_N)_{\text{tot}}$ and C_A can be obtained.

$$(C_N)_{\text{tot}} = \frac{2W_C + m_L g - 2q_\infty S_{\text{ref}}C_A \cos\,\Phi}{2q_\infty S_{\text{ref}} \sin\,\Phi} \qquad (42)$$

Breathing Mode: Parachutes are made using flexible materials and are inherently non-rigid objects. As they deform during flight, the projected reference area S_{proj} changes and affects the axial motion of the system. Reference [1] describes this axial oscillatory behavior as the "breathing mode." Flight test data showed that during the breathing mode as the canopies contracted from the

nominal reference area, V_{down} increased; conversely, as the canopies increased from the nominal reference area, V_{down} decreased.

The underlying dynamics of the breathing mode are straightforward and can be represented by Equations (43) through (45). The parameter η is used to approximate the deformation of the parachute away from its nominal projected area. The oscillatory deformation behavior can be represented by a second-order harmonic oscillator. The natural frequency, ω_n, is dependent on many parameters (e.g., the parachute material properties, porosity, natural environments).

$$\ddot{\eta} + d\dot{\eta} + \omega_n^2 \eta = 0 \qquad (43)$$

The C_A consists of a baseline term and a term dependent on η:

$$C_A = C_{A_0} + C_{A_\eta} \eta \qquad (44)$$

The equation of motion in the down direction is

$$\left(m_L + 2m_{C,\mathrm{dry}}\right)\dot{w} = S_{\mathrm{ref}}\rho w^2 C_A + \\ \left(m_L + 2m_{C,\mathrm{dry}}\right)g \qquad (45)$$

where $m_{C,\mathrm{dry}}$ is the dry mass of the parachutes and w is the velocity in the down direction.

Conclusions: The overall motion of a system containing two parachutes and a capsule is extremely complicated with nonlinearities and flexibility effects. It is usually difficult to obtain insight into the fundamental dynamics of the system by examining results from a multibody simulation based on nonlinear equations of motion. In the current work, the dynamics of the scissors, maypole, breathing, and pendulum modes observed during various drop tests is studied on an individual basis by using a simplified dynamics model for each mode. Analysis of the flight data shows that the scissors and maypole modes are largely dominated by proximity aerodynamics. The separate studies of each mode produce compatible results and provide a better understanding of the behavior of the complex multi-body system.

References:

[1] Ali, Y., Sommer, B., Troung, T., Anderson, B., and Madsen, C., "Orion Multi-Purpose Crew Vehicle Solving and Mitigating the Two Main Cluster Pendulum Problem," No. 2017-4056, *24rd Aerodynamic Decelerator Conference*, AIAA, 2017.

[2] Ray, E. S., and Machín, R. A., "Pendulum Motion in Main Parachute Clusters," No. 2015-2138, AIAA, 2015.

[3] Etkins, B., *Dynamics of Atmospheric Flight*, Dover Publications, Mineola, NY. 2000.

[4] White, F. M., and Wolf, D. F., "A Theory of Three-Dimensional Parachute Dynamic Stability," *Journal of Aircraft*, Vol. 5, No. 1, 1968, pp. 86–92.

[5] Ginn, J. M., Clark, I. G., and Braun, R. D., "Parachute Dynamic Stability and the Effects of Apparent Inertia," No. 2014-2390, AIAA, 2014.

[6] Knacke, T. W., *Parachute Recovery Systems Design Manual*, Para Publications, Santa Barbara, 1991.

[7] Greathouse, J., and Schwing, A., "Study of Geometric Porosity and Drag using Computational Fluid Dynamics for Rigid Parachute Shapes," No. 2015-2131, *23rd Aerodynamic Decelerator Conference*, AIAA, 2015.

[8] Wolf, D., and Heindel, K., "A Steady Rotation Motion for a Cluster of Parachutes," No. 2005-1629, AIAA, 2005.

[9] Roithmayr, C. M., Beaty, J., Pei, J., Barton, R. L., and Matz, D. A., "Linear Analysis of Two-Parachute System Undergoing Pendulum Motion," submitted, 25th Aerodynamic Decelerator Conference, AIAA, 2019.

[10] Pei, J., "Nonlinear Analysis of a Two-Parachute Cluster System Undergoing Pendulum Motion," submitted, 25th Aerodynamic Decelerator Conference, AIAA, 2019.

[11] Pamadi, B. N., *Performance, Stability, Dynamics, and Control of Airplanes*, 3rd Ed, AIAA, 2015, pp. 427-428.

[12] Kane, T.R., and Levinson, D. A., Dynamics: Theory and Application, McGraw-Hill, New York, 1985, pp. 45 – 50, 158-159.